Available online at www.sciencedirect.com
SCIENCE DIRECT
Journal of Catalysis 241 (2006) 74–82
JOURNAL OF CATALYSIS
www.elsevier.com/locate/jcat

Oxidation of methane over a Rh/Al_2O_3 catalyst using microfabricated reactors with integrated heating

Osnat Younes-Metzler [a,1], Johnny Johansen [b], Sune Thorsteinsson [c], Søren Jensen [c], Ole Hansen [c], Ulrich J. Quaade [a,*]

[a] *Danish Research Foundation's Center for Individual Nanoparticle Functionality (CINF), NanoDTU, Department of Physics, Technical University of Denmark, 2800 Kgs. Lyngby, Denmark*

[b] *Department of Chemical Engineering, Technical University of Denmark, 2800 Kgs. Lyngby, Denmark*

[c] *Danish Research Foundation's Center for Individual Nanoparticle Functionality (CINF), NanoDTU, MIC – Department of Micro and Nanotechnology, Technical University of Denmark, 2800 Kgs. Lyngby, Denmark*

Received 22 December 2005; revised 7 April 2006; accepted 15 April 2006

Available online 30 May 2006

Abstract

Microfabricated reactors with integrated local heating were fabricated for investigating fast exothermic reactions with independent control of temperature and flow rate. As an example, oxidation of methane over a supported rhodium catalyst was investigated. The reaction was studied at different oxygen-to-methane ratios, covering both fuel-lean and fuel-rich compositions with full and partial oxidation. Good agreement with previously reported results indicates that the microfabricated reactors are useful for studying fast exothermic reactions.

Keywords: Microreactors; Partial oxidation; Methane

1. Introduction

Microfabricated reactors [1–4] have numerous advantages over more traditional reactors. These advantages are direct consequences of the small dimensions of the reactor. For example, the corresponding large surface-to-volume ratio implies superior heat dissipation and control of temperature, and the small channel dimensions ensure a low Reynolds number with well-defined laminar flow for realistic flow rates. The small size also enhances quenching of free radicals, which, together with the good heat dissipation, effectively suppresses gas-phase reactions in flammable or explosive gas mixtures. Even if an explosion should occur in the reactor, the small volume will make it harmless. Further, the small reactors respond quickly to variations in reaction conditions, increasing the throughput in the experimental setup. Together, these advantages make the microfabricated reactors ideal for studies of fast exothermic reactions, where it is difficult to vary, for example, temperature and flow rate independently due to the extensive self-heating from the reactions and where safety is an important issue if reactants are not diluted in inert gases.

In a recent paper, we described a high-temperature microreactor setup for studying partial oxidation reactions using microfabricated silicon reactors [5]. In the present paper, we further develop this experimental setup, now including an integrated heating element, which enables local heating of the catalyst bed and provides even better temperature control of the reaction zone.

To test the performance of the reactor, both partial and full oxidation of methane over 0.1 wt% Rh/Al_2O_3 catalysts under fuel-rich and fuel-lean conditions are studied in the microfabricated reactor, with emphasis on partial oxidation. This reaction system is chosen because the mixture of oxygen and methane is potentially explosive, the reactions are fast and exothermic (developing a lot of heat), and the system itself is interesting for production of synthesis gas [6].

* Corresponding author.
E-mail addresses: osnat@nano.ku.dk (O. Younes-Metzler), quaade@fysik.dtu.dk (U.J. Quaade).
[1] Current address: Nano-Science Center, University of Copenhagen, Universitetsparken 5, DK-2100 Copenhagen, Denmark.

0021-9517/$ – see front matter
doi:10.1016/j.jcat.2006.04.014

The production of synthesis gas (syngas) is a step in the indirect conversion of methane to liquid fuel. The conversion of methane to liquid fuel is of great importance in the utilization of natural gas resources, and both direct and indirect routes have been suggested. The indirect routes require conversion of methane to syngas, which can then be converted to liquid fuel by a Fischer–Tropsch reaction [7] or methanol synthesis [8,9]. Conversion of methane to syngas through catalytic partial oxidation is mildly exothermic ($CH_4 + (1/2)O_2 \rightarrow 2H_2 + CO$, $\Delta H = -36$ kJ/mol), producing syngas with an H_2/CO ratio ($\leqslant 2$) suitable for both the Fischer–Tropsch reaction and methanol synthesis. The reaction is fast, with full conversion measured even at millisecond contact times. This causes high heat generation in the reactor at high flow rates, thus making it difficult to study the reaction's dependence on temperature and flow rate independently. For the partial oxidation reaction, supported noble metal catalysts, including Rh, Ru, Pd, and Pt [10–12], as well as supported Ni catalysts, have been used [13,14]. Among these catalysts, rhodium is considered the most reactive, with a high and stable syngas yield [11].

The literature includes numerous experimental studies [15–20] as well as model development and comparison between model and experimental data [21–26]. Various reaction pathways have been suggested [27–30], and the studies have revealed a good understanding of the process with respect to ignition behavior, selectivity, influence of contact times and gas composition, and other factors. In microstructured reactors, partial oxidation of methane has been performed in a metallic multichannel reactor made entirely of rhodium [31], and partial oxidation of propane has been performed in multichannel metallic reactors impregnated with porous Rh-catalysts [32,33].

In the present work, many of the previously obtained results are reproduced to confirm the function of the microreactor. The reaction rate is measured as a function of the fuel-to-air ratio, and the ignition temperature (at which the partial oxidation reaction starts) is identified for each fuel-to-air ratio. For full oxidation, the apparent activation energy is determined. At temperatures above the ignition temperature, where partial oxidation contributes to the reaction, the gas composition is limited mostly by equilibrium, and the measured gas compositions are compared with calculated equilibrium compositions. To investigate the transition between kinetic limitation and equilibrium limitation, measurements at varying contact times are performed.

2. Experimental

The microreactor used in the present study is similar to that used in a previous study [5], with the important difference that the present reactor contains an integrated electrical heating element, which significantly reduces the thermal response time of the system. The microreactor is shown in Fig. 1. The gas channels, located on the front of the microreactor (Fig. 1a), consist of two inlet channels, a reaction chamber in which a catalyst is placed, and one outlet channel. The two inlet channels make on-chip mixing of oxygen and methane possible, thereby minimizing the volume of the potentially explosive gas mixture.

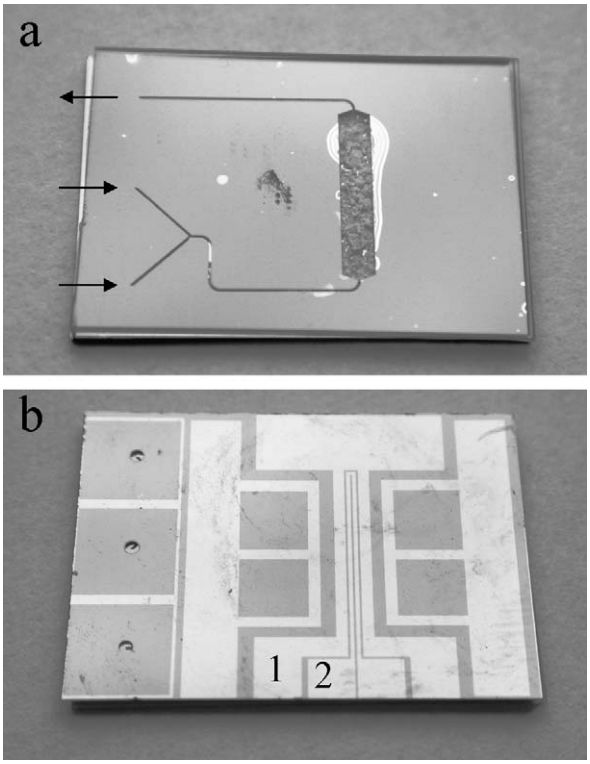

Fig. 1. Microreactor layout: (a) front, (b) back. The integrated heating element is indicated by 1 and the integrated temperature sensor is indicated by 2.

This has been demonstrated to be a safe way to study the reaction [5]. The reactor is sealed with a Pyrex glass lid. The heating element is located on the back of the microreactor (Fig. 1b), along with access ports for the inlet and outlet channels.

Using an integrated heating element significantly reduces the system's response time compared with earlier versions, in which the heater was in the form of a 525 μm thick piece of silicon located on top of the Pyrex lid. In the current reactors, the integrated heating element is a thin-film conductor located directly underneath the catalyst bed with only 20–50 μm of silicon and 200 nm of SiO_2 separating them. The time constant for heat to propagate through such a layer is on the order of microseconds. The low mass of the integrated heating element itself reduces the amount of heat stored in the system and thus reduces the heating and cooling time constants. Heating and cooling rates exceeding 100 °C/s can be easily obtained. The heating element comprises a 500 nm thick layer of nickel disilicide ($NiSi_2$), which is compatible with temperatures up to 960 °C.

The microreactors are fabricated using silicon micromachining methods. The heaters are realized by reacting a lift-off structured nickel layer with an underlying polycrystalline silicon layer by annealing them at 850 °C. Thereafter, the remaining silicon is removed by KOH wet etching, ensuring lateral electrical insulation at elevated temperatures, at which silicon becomes conducting. The finished heater structures are insulated from the silicon substrate by a previously grown SiO_2 layer. After the heaters are fabricated, the access ports and channel structures are etched from the back and front of the substrate, respectively, using deep reactive ion etching. Finally, after cata-

lyst deposition in the reactor chamber, a Pyrex lid is anodically bonded to the reactor to seal the channel system.

The catalyst deposition procedure is identical to the sol–gel technique described previously [5]. First, alumina gel is deposited in the reactor channel while the reactor temperature is maintained at 80 °C. When the desired amount of material is deposited, the reactor is calcined at 400 °C for 30 min. The resulting porous alumina (usually 130 m^2/g) is then impregnated with active material—in this case rhodium-acetyleacetonate—to obtain Rh(0.1 wt%)/Al_2O_3.

The temperature is measured from the Pyrex side using an IR sensor focused to a spot size of 1 mm on the reactor. Because of its small thickness, the Pyrex lid is somewhat transparent to IR radiation, meaning that the measured temperature is an average over the lid and catalyst bed temperatures. This gives the possibility of detecting step changes of the temperature of the catalyst surface associated with ignition/extinction of the reaction. The IR sensor is calibrated by making simultaneous IR and thermocouple recordings using a thermocouple inserted into the reactor channel of a reactor in which one end has been broken off. The absolute accuracy is estimated to ±20 °C, and the sensitivity is 0.2 °C. Measurements performed with a thermocamera show that the temperature is uniform within 1 °C over >90% of the reaction zone and does not vary more than a few percentage points along the complete reaction zone. Because of the local heating of the reaction zone and the efficient heat dissipation, very little heat propagates to other parts of the chip, resulting in temperatures below 200 °C in the inlet and outlet access port regions over the entire range of working temperatures. This enables the use of Viton O-rings for the seal between the microreactor and the interfacing, which is a significant advantage over the previous use of gold O-rings [5]. The quality of the seal is improved, and the handling is much easier when using Viton O-rings.

The gas flow through the reactor is controlled by mass flow controllers, and gas analysis is done with a mass spectrometer. Argon is added to the gas mixture to keep the total flow through the microreactor constant. Argon is also used as an internal standard. This is especially important for the partial oxidation reaction, in which the reaction generates an increase in the total number of moles. Calibration factors for all gases are measured separately. With the experimental setup, it is not possible to measure the water signal reliably, because the maximum temperature in the chamber of the mass spectrometer is limited to around 70 °C. At this temperature, water condenses at the chamber surfaces, causing an error in the measured water concentration; therefore, this is not used.

The oxidation of methane is studied under both fuel-rich and fuel-lean conditions. Instead of using the conventional stoichiometric ratio, $\phi = \%CH_4/\%O_2$, we use the modified stoichiometric ratio, $\Phi = \phi/(\phi + 1)$ [34]. The modified ratio has the advantage of being limited to the range 0–1 and symmetric around the stoichiometric point of 0.5. Throughout this paper, the term "stoichiometric ratio" refers to this modified stoichiometric ratio.

The catalyst used in all experiments is 0.1 wt% Rh/Al_2O_3. The total gas flow in all experiments is 4.5 mL/min, giving a residence time of approximately 60 ms. The oxidation of methane is studied in the temperature range of 300–700 °C. The temperature is increased manually in steps of approximately 15 °C by increasing the current in the heating element. After steady state is reached, the temperature and gas composition are recorded. Because of the rapid response of the complete system, steady state is reached in about 1 min, and the complete measurement is carried out in about 20 min.

3. Equilibrium calculations

Once the ignition temperature is reached, all of the oxygen is consumed in the reactions. At this point, the reaction changes from being kinetically limited to a state where it can be limited by both equilibrium and kinetics. Assuming that the reaction approaches equilibrium, changes in concentrations with temperature correspond to an altered equilibrium composition. To test this, the equilibrium composition of the reaction gas has been calculated as function of temperature and compared with the measured concentrations.

The equilibrium calculations have been done by the method developed by Michelsen [35], which minimizes the total Gibbs free energy of a multicomponent mulitiphase system at constant pressure and temperature. This method has been modified so that it includes fugacity coefficients to account for nonideal behavior. The thermodynamic data needed for the calculations are obtained from published data sources [36,37].

4. Results and discussion

Fig. 2 shows a typical methane oxidation experiment together with the calculated equilibrium composition. The experiment is performed under fuel-rich conditions ($\Phi = 0.7$). At low temperatures, the methane is converted mainly to CO_2 and H_2O. As the temperature of the reactor reaches a critical value (in this case 590 °C), the H_2 and CO signals suddenly appear, and the CO_2 signal decreases. This critical temperature is known as the ignition temperature of the reaction [34]. This demonstrates that at low temperatures, only the full oxidation reaction occurs, whereas at high temperatures, both the full and partial oxidation reactions occur. The ignition of the partial oxidation reaction is also seen as a sharp increase in the conversion of methane and the total consumption of oxygen. With a further temperature increases, the conversion of methane and the concentrations of the partial oxidation products CO and H_2 increase, and the concentration of CO_2 decreases. Similar behavior has been observed in an earlier study [19].

Because all of the oxygen has reacted at temperatures above the ignition temperature, the partial oxidation reaction might be limited by the thermodynamic equilibrium, rather than by surface kinetics or mass transport. Increasing the temperature further after ignition then shifts the equilibrium concentrations, resulting in increased methane conversion. The calculated equilibrium concentrations of the different gas components in the outlet gas are represented by the solid lines in Fig. 2. The calculations fit well with the measured concentrations and show that in this case, the reaction proceeds close to equilibrium.

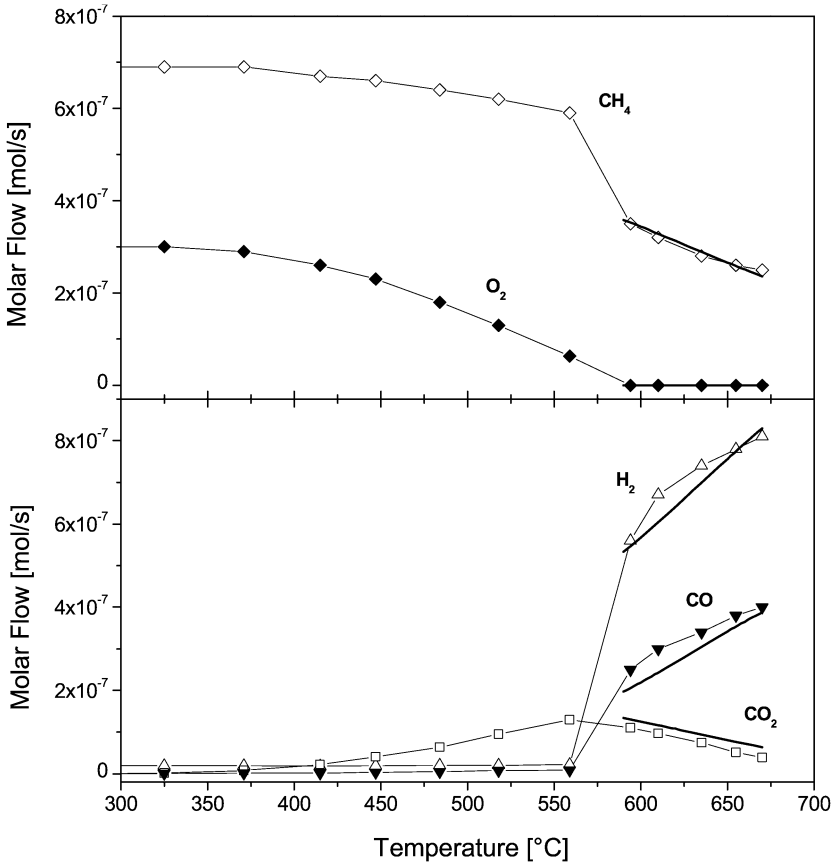

Fig. 2. Outlet molar flow of the different gas species as a function of temperature. Experimental data are displayed as symbols and solid lines show calculated equilibrium data.

Fig. 3 shows the conversion of methane as a function of temperature for different stoichiometric ratios. It is clearly seen that the conversion of methane increases with increasing temperature for all methane-to-oxygen ratios. Under fuel-lean conditions, the full oxidation reaction is the main reaction, and no ignition is seen in the studied temperature range, except when $\Phi = 0.45$. Under fuel-lean conditions, the conversion of methane depends only slightly on Φ and reaches about 35% conversion at around 625 °C.

Under fuel-rich conditions below the ignition temperature, the methane conversion depends only weakly on Φ, as in the fuel-lean case. But above the ignition temperature, methane conversion is strongly dependent on Φ, as was also observed previously [17]. This finding is expected, because the reaction is limited by oxygen, and less oxygen in the inlet gas will result in a lower conversion rate of methane. To illustrate this, Fig. 4 shows the methane conversion as a function of Φ for four different temperatures along with the corresponding equilibrium calculations. The measured data and calculated curves closely agree and demonstrate an increased equilibrium conversion of methane with increasing temperature and decreasing stoichiometric ratio Φ.

Another feature illustrated in Fig. 3 is the variation of ignition temperature with Φ. Fig. 5 provides a plot of the ignition temperature as function of Φ. The ignition temperatures are in the range of 450–650 °C and decrease with increasing methane-to-oxygen ratio. Similar observations have been reported by Veser et al. [34], who explained this decrease in ignition temperature as a result of competitive adsorption of methane and oxygen. At low temperatures, the surface of the catalyst is almost completely covered with oxygen. As the temperature of the catalyst is increased, desorption of oxygen starts, thereby creating free sites for methane to adsorb and allowing surface reaction to take place. As the partial pressure of oxygen decreases with increasing Φ, the critical CH_4/O_2 surface ratio needed for surface ignition can be reached at lower temperatures. A simplified model describing competitive adsorption of hydrocarbon species and oxygen has been analyzed, giving the following relation between the stoichiometry and temperature at ignition [34]:

$$\Phi = \phi/(1+\phi), \quad \phi = aT^2 \exp(E_{\text{app}}/RT),$$

where T is the ignition temperature, E_{app} is the apparent activation energy, R is the gas constant, and a is a proportionality factor. Fig. 5 plots this expression for $a = 4 \times 10^{-11}$ K^{-2} and $E_{\text{app}} = 80$ kJ/mol and shows that it fits the data well. For comparison, a value of $E_{\text{app}} \approx 110$ kJ/mol has been found for methane oxidation on platinum [34].

Arrhenius-type plots are created for different fuel-to-oxygen ratios based on the total conversion of methane as a function of temperature. Under fuel-lean conditions, a single linear regime is observed for each Φ. Under fuel-rich conditions, two linear

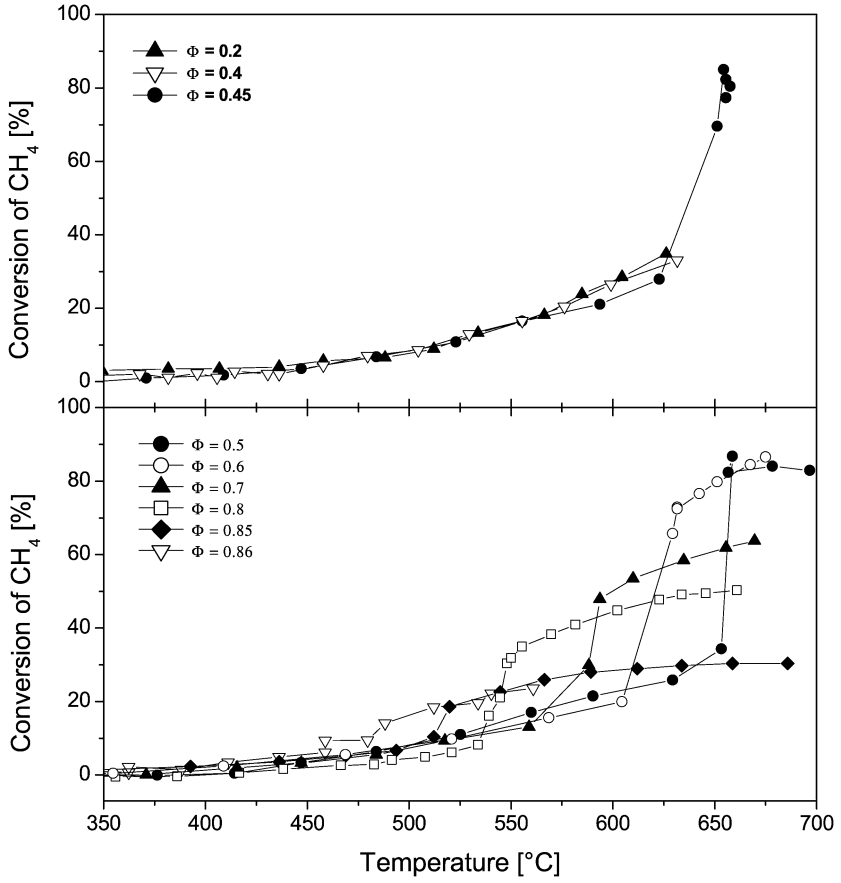

Fig. 3. The measured conversion of methane as a function of the temperature for different stoichiometric ratios Φ.

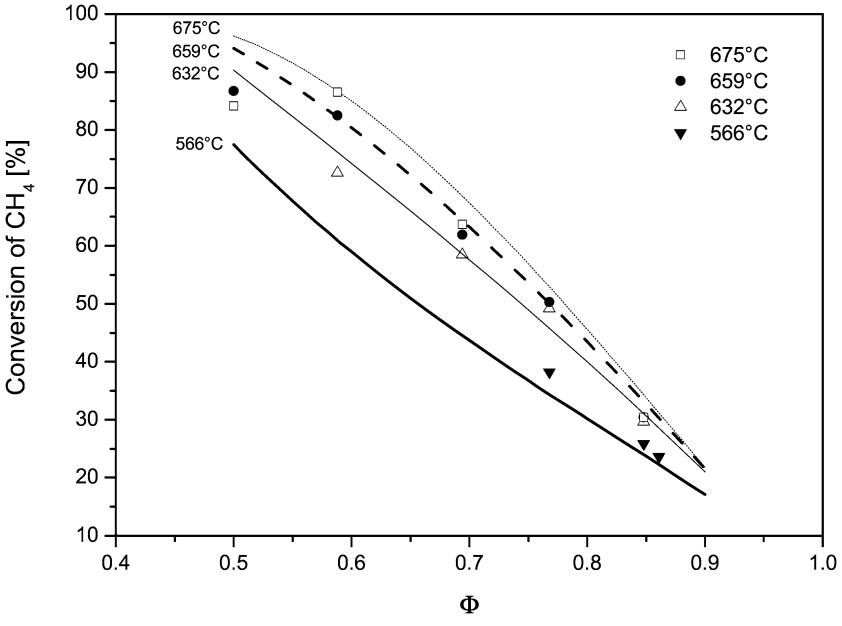

Fig. 4. The conversion of methane as a function of the stoichiometric ratio Φ at different temperatures. Experimental data are displayed as symbols and solid curves show calculated equilibrium data.

regions are observed, as shown in Fig. 6: one region at temperatures below ignition, corresponding to the full oxidation reaction, and a second region at temperatures above ignition, corresponding to the partial oxidation reaction.

In the case of full oxidation, the reaction is kinetically limited, and the slope can be interpreted as apparent activation energy. Apparent activation energies determined for the different methane-to-oxygen ratios are shown in Fig. 7A. Although

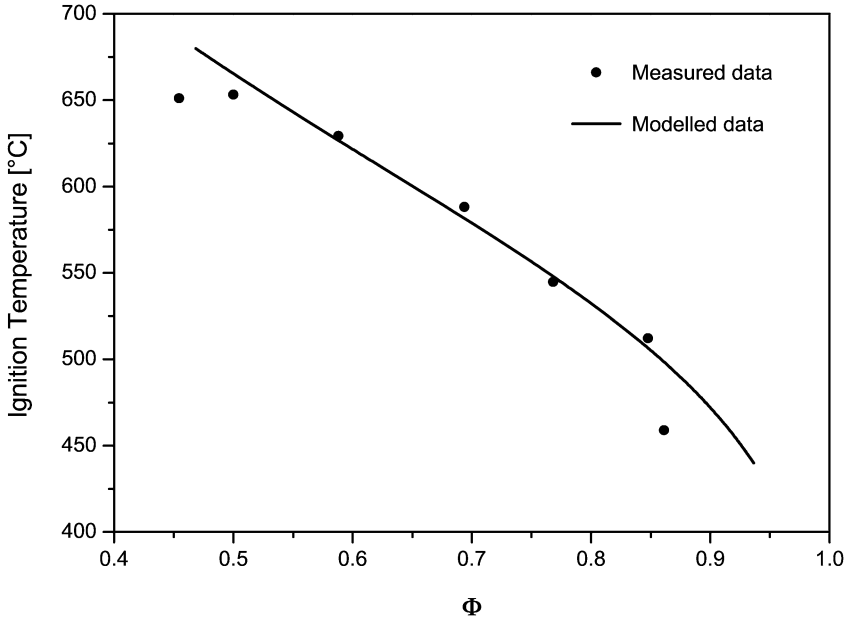

Fig. 5. The ignition temperature as a function of the stoichiometric ratio Φ. Symbols are experimental data and the solid curve is a model adapted from [34].

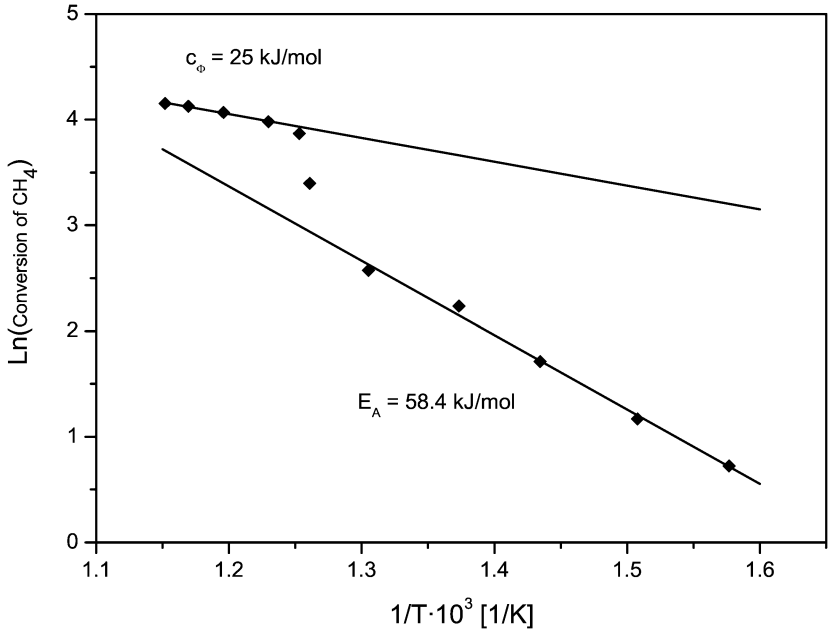

Fig. 6. Arrhenius-type plot for the stoichiometric ratio $\Phi = 0.7$. Two linear regions are observed. At temperatures below ignition the slope reflects an apparent activation energy E_A. Above ignition the slope determines the temperature coefficient c_Φ in the temperature dependent equilibrium.

the data are scattered, the apparent activation energy seems to decrease with increasing Φ, from $E_A = 65$ kJ/mol at $\Phi = 0.2$ to $E_A = 45$ kJ/mol at $\Phi = 0.85$. Lower oxygen content in the inlet gas lowers the activation energy for full oxidation.

In the case of partial oxidation, the conversion of oxygen is almost complete, and the process might become limited by thermodynamic equilibrium rather than by surface kinetics or by a combination of the two factors. Therefore, this linear part of the Arrhenius plot cannot be interpreted as activation energy, but is related to the overall temperature-dependent equilibrium of the different reactions occurring at temperatures above ignition. To test whether this linear part can be assigned to equilibrium alone, a comparison is made to the calculated equilibrium; the appearance of straight lines for the methane conversion in an Arrhenius-like plot in the equilibrium-limited temperature region above ignition indicates that the equilibrium concentration of methane changes with temperature as $\exp(-c_\Phi/RT)$, where c_Φ is a temperature coefficient. Fig. 7B shows the measured temperature coefficients as a function of Φ. In the temperature range investigated, the calculated equilibrium concentration of methane can also be fitted to an Arrhenius-type expression to get a prediction for the temperature coefficient. This prediction, shown in Fig. 7B, fits well with the measured values. Both the predicted and measured values show significant changes in the

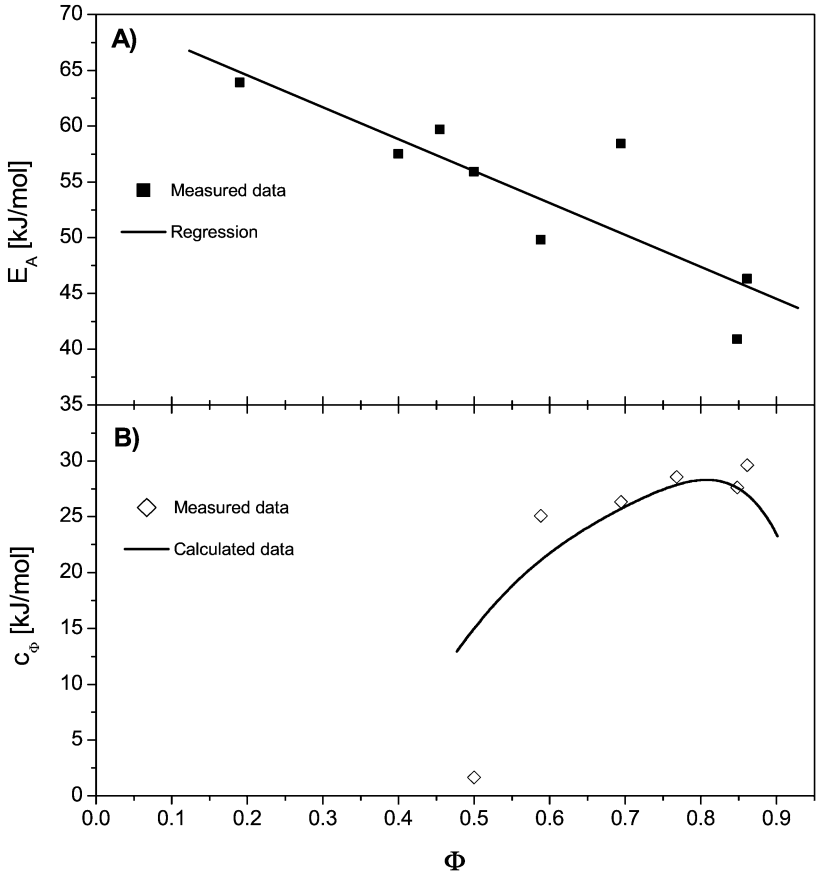

Fig. 7. (A) The apparent activation energy for the full oxidation reaction as a function of the stoichiometric ratio Φ. (B) The equilibrium temperature coefficient c_Φ as a function of Φ.

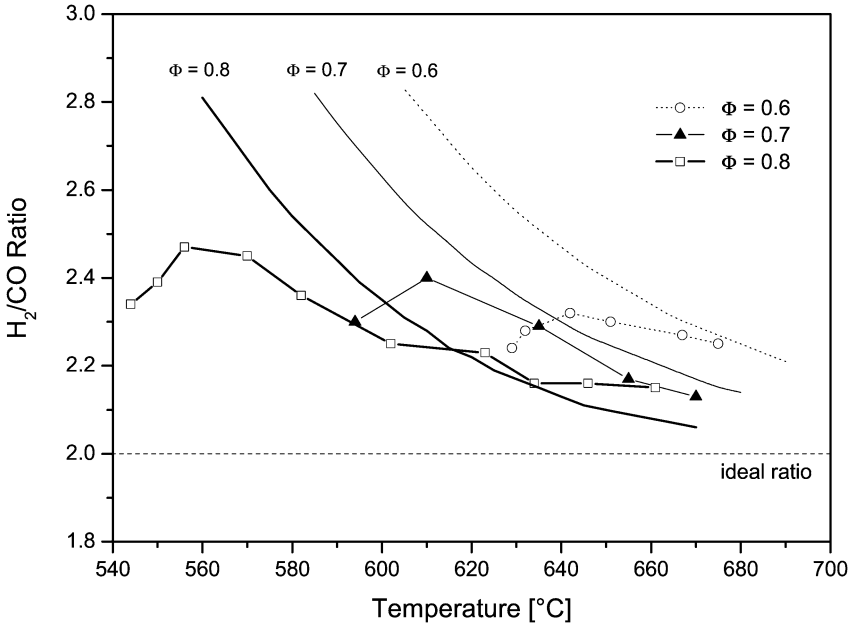

Fig. 8. The outlet H_2/CO ratio as a function of the temperature for different values of the stoichiometric ratio Φ. Experimental data are displayed as symbols and solid curves show calculated equilibrium data.

equilibrium around $\Phi = 0.5$. Again, this indicates that equilibrium is approached in the reactor.

Fig. 8 shows the H_2/CO ratio, which is important when using the product gas for further synthesis, as a function of temperature for the different Φ's. After ignition (lowest temperature plotted for each Φ), the ratio first increases and then approaches 2 in a seemingly asymptotic way. The higher the Φ, the lower the temperature required for obtaining ratios close to 2. The

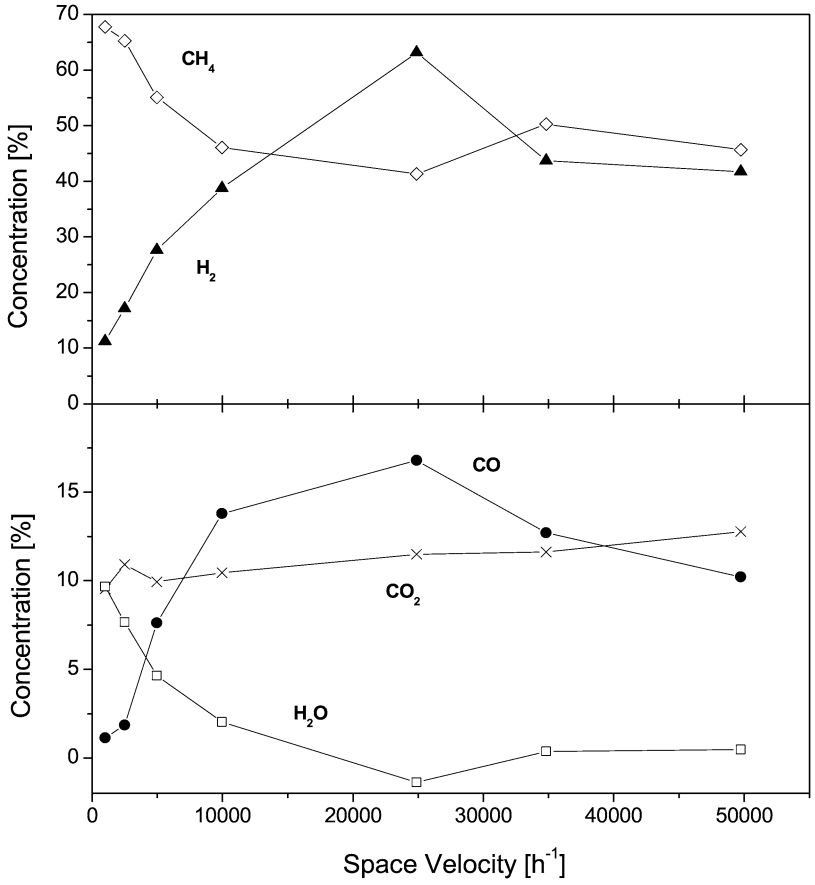

Fig. 9. Outlet composition as function of total flow rate for $\Phi = 0.8$ and a temperature of 570 °C. Data from water are calculated from the mass balance.

curves represent the predicted H_2/CO ratio as determined by the equilibrium calculations. At lower temperatures, the predicted equilibrium H_2/CO ratio deviates significantly from the measured ratio, indicating that equilibrium is not reached at the lower temperatures close to the ignition temperature. To address this further, the flow was varied for $\Phi = 0.8$ at a constant temperature of 570 °C, which is close to but above ignition. As shown in Fig. 9, the conversion of CH_4 and the selectivity toward H_2 and CO increase with space velocity up to 2.5×10^4 h^{-1}, then flatten or even decrease slightly. At low temperatures, the calculated equilibrium is shifted toward production of H_2O and CO_2, with very limited production of H_2 and CO. This is clearly shown in Fig. 9 at low flow rates. At higher flow rates, the composition moves away from equilibrium, the conversion of CH_4 increases, and production of CO and H_2 is greatly increased. This is in qualitative agreement with a previous model [21] that predicts that at relatively low space velocities, the conversion of CH_4 and selectivity toward H_2 will increase with space velocity. This increase, caused by the kinetics of the reaction, illustrates the benefits of using rhodium catalysts for efficient syngas production at low temperatures.

Finally, the temperature during ignition and extinction was closely monitored to detect any possible change in temperature caused by heat developed by the chemical reaction. Ignition is reached by increasing the temperature at a slow, steady rate, and extinction is accomplished by shutting off the oxygen flow. The IR sensor was first focused close to the inlet of the reactor, and subsequently the experiment was repeated with the sensor focused on the middle of the reactor. In the middle of the reactor, a small temperature increase (<1 °C) was observed at ignition, but close to the inlet, no abrupt temperature change was observed. This is in contrast to previous results for a larger reactor [16], in which significant heating of the catalyst surface was observed. The difference is probably due to the improved thermal properties of the microfabricated reactor, in which heat was applied externally to maintain a high temperature, compared with the earlier study [16] in which heat came from the chemical reaction, which is self-sustained. In all of the measurements, the heat generated chemically inside the reactor is <0.1 W, which should be compared with the 40 W applied to maintain the high temperature. This demonstrates that the heat is effectively dissipated and that flow rate and temperature can be varied independently.

5. Conclusion

Microfabricated reactors with integrated local heating of the reaction zone have been fabricated and investigated thermally. As an example, the partial oxidation of methane over rhodium was investigated. Our results agree well with earlier studies and demonstrate that flow rate and reactor temperature can be varied independently. At low flow rate or high temperature, the reaction in the microfabricated reactor approached equilibrium,

whereas at high flow rate or low temperature, the reaction was kinetically limited with high selectivity toward hydrogen, as reported previously. Our findings demonstrate that the microfabricated reactor is convenient and reliable for studying fast exothermic reactions.

Acknowledgments

The authors thank the STVF for financial support. CINF is sponsored by The Danish National Research Foundation. S.J. is supported by the Danish Research Council for Technology and Production Sciences.

References

[1] K.F. Jensen, Chem. Eng. Sci. 56 (2001) 293.
[2] G. Kolb, V. Hessel, Chem. Eng. J. 98 (2004) 1.
[3] K. Jähnisch, V. Hessel, H. Löwe, M. Baerns, Angew. Chem. Int. Ed. 43 (2004) 406.
[4] L. Kiwi-Minsker, A. Renken, Catal. Today 110 (2005) 2.
[5] O. Younes-Metzler, J. Svagin, S. Jensen, C.H. Christensen, O. Hansen, U.J. Quaade, Appl. Catal. A: General 284 (2005) 5.
[6] D.A. Hickman, L.D. Schmidt, Science 259 (1993) 343.
[7] G.P. Van der Laan, A.A.C.M. Beenachers, Catal. Rev. Sci. Eng. 41 (1999) 255.
[8] F.J. Keil, Microporous Mesoporous Mater. 29 (1999) 49.
[9] P. Reubroycharoen, T. Yamagami, T. Vitidsant, Y. Yoneyama, M. Ito, N. Tsubaki, Energy Fuels 17 (2003) 817.
[10] P.M. Witt, L.D. Schmidt, J. Catal. 163 (1996) 465.
[11] P.M. Torniainen, X. Chu, L.D. Schmidt, J. Catal. 146 (1994) 1.
[12] M. Lyubovsky, L.L. Smith, M. Castaldi, H. Karim, B. Nentwick, S. Etemad, R. LaPierre, W.C. Pfefferle, Catal. Today 83 (2003) 71.
[13] D. Dissanayake, M.P. Rosynek, J.H. Lunsford, J. Phys. Chem. 97 (1993) 3644.
[14] V.R. Choudhary, A.M. Rajput, B. Prabhakar, J. Catal. 139 (1993) 326.
[15] A.T. Ashcroft, A.K. Chetham, J.S. Foord, M.L.H. Green, C.P. Grey, A.J. Murrell, P.D.F. Vernon, Nature 344 (1990) 319.
[16] L. Basini, A. Guarinoni, A. Aragno, J. Catal. 190 (2000) 284.
[17] D.A. Hickman, E.A. Haupfear, L.D. Schmidt, Catal. Lett. 17 (1993) 223.
[18] P.M. Witt, L.D. Schmidt, J. Catal. 163 (1996) 465.
[19] J.-D. Grunwaldt, L. Basini, B.S. Clausen, J. Catal. 200 (2001) 321.
[20] K.L. Hohn, L.D. Schmidt, Appl. Catal. A 211 (2001) 53.
[21] M. Bizzi, G. Saracco, R. Schwiedernoch, O. Deutschmann, AIChE J. 50 (2004) 1289.
[22] A.B. Mhadeshwar, D.G. Vlachos, J. Chem. Phys. B 109 (2005) 16819.
[23] D.G. Vlachos, L.D. Schmidt, R. Aris, AIChE J. 40 (1994) 1018.
[24] C. Appel, J. Mantzaras, R. Schaeren, R. Bombach, A. Inauen, N. Tylli, M. Wolf, T. Griffin, D. Winkler, R. Carroni, Proc. Combust. Inst. 30 (2005) 2509.
[25] O. Deutschmann, F. Behrendt, J. Warnatz, Catal. Today 46 (1998) 155.
[26] R. Schwiedernoch, S. Tischer, C. Correa, O. Deutschmann, Chem. Eng. Sci. 58 (2003) 633.
[27] M. Prettre, C. Eichner, M. Perrin, J. Chem. Soc., Faraday Trans. 43 (1946) 335.
[28] D.A. Hickman, L.D. Schmidt, J. Catal. 138 (1992) 267.
[29] O.V. Buyevskaya, D. Wolf, M. Baerns, Catal. Lett. 27 (1994) 131.
[30] H.Y. Wang, E. Ruckenstein, Catal. Lett. 59 (1999) 121.
[31] M. Fichtner, J. Mayer, D. Wolf, K. Schubert, Ind. Eng. Chem. Res. 40 (2001) 3475.
[32] I. Aartun, T. Gjervan, H. Venvik, O. Görke, P. Pfeifer, M. Fathi, A. Holmen, K. Schubert, Chem. Eng. J. 101 (2004) 93.
[33] I. Aartun, H.J. Venvik, A. Holmen, P. Pfeifer, O. Görke, K. Schubert, Catal. Today 110 (2005) 98.
[34] G. Veser, M. Ziauddin, L.D. Schmidt, Catal. Today 47 (1999) 219.
[35] M.L. Michelsen, Fluid Phase Equilib. 53 (1989) 73.
[36] I. Barin, Thermodynamic Data of Pure Substances, VCH, Weinheim, 1989.
[37] O. Knacke, O. Kubaschewski, K. Hesselmann, Thermodynamic Properties of Inorganic Substances, second ed., Springer, Berlin, 1991.